

PAPER • OPEN ACCESS

## Tunable, few-cycle, CEP-stable mid-IR optical parametric amplifier for strong field applications

To cite this article: Mikayel Musheghyan *et al* 2020 *J. Phys. B: At. Mol. Opt. Phys.* **53** 185402

View the [article online](#) for updates and enhancements.

You may also like

- [Advances in laser technology for isolated attosecond pulse generation](#)  
C Vozzi, F Calegari, F Ferrari *et al.*
- [Special issue on optical parametric processes](#)  
Guest editors, Jeffrey Moses, Oliver D Mücke *et al.*
- [Generation of ultrashort pulses by four wave mixing in a gas-filled hollow core fiber](#)  
Anna G Ciriolo, Aditya Pusala, Matteo Negro *et al.*

# Tunable, few-cycle, CEP-stable mid-IR optical parametric amplifier for strong field applications

Mikayel Musheghyan<sup>1</sup>, Prabhash Prasannan Geetha<sup>2</sup> ,  
Davide Faccialà<sup>2</sup> , Aditya Pusala<sup>2</sup>, Gabriele Crippa<sup>2,3</sup>, Andrea Campolo<sup>3</sup>,  
Anna G Ciriolo<sup>2</sup> , Michele Devetta<sup>2</sup> , Andreas Assion<sup>1</sup>,  
Cristian Manzoni<sup>2</sup>, Caterina Vozzi<sup>2,4</sup>  and Salvatore Stagira<sup>2,3</sup>

<sup>1</sup> High Q Laser GmbH, Vienna, Austria and University of Kassel, Institute of Physics, Kassel, Germany

<sup>2</sup> Istituto di Fotonica e Nanotecnologie, CNR, Italy

<sup>3</sup> Dipartimento di Fisica, Politecnico di Milano, Italy

E-mail: [caterina.vozzi@cnr.it](mailto:caterina.vozzi@cnr.it)

Received 18 March 2020, revised 29 May 2020

Accepted for publication 29 June 2020

Published 22 July 2020



## Abstract

We present a robust, three-stage optical parametric amplifier driven by a Ti:Sapphire ultrafast laser system that implements passive carrier-envelope phase stabilization and directly generates five-cycle mid-IR pulses by dispersion compensation. The source is based on potassium titanyl arsenate crystals and exploits intra-pulse difference-frequency seed generation in the mid-IR. This source will be particularly suited for applications in strong-field physics, such as high order harmonic generation and photoelectron spectroscopy.

Keywords: optical parametric amplifier, high order harmonic generation, nonlinear optics

(Some figures may appear in colour only in the online journal)


## 1. Introduction

The last decades have seen substantial progress in the development of optical parametric amplifiers (OPAs) in the 2.5–5  $\mu\text{m}$  spectral region (hereafter mid-IR). Various applications of mid-IR ultrashort pulses have been reported, ranging from pump-probe spectroscopy [1] to nonlinear optics [2], atmospheric sensing [3], bio-sciences [4], high harmonic generation (HHG) in solids [5] and gases [6] as well as laser-induced electron diffraction in molecules [7]. In the case of HHG, the cut-off frequency of the harmonic spectrum scales as  $\lambda_d^2$ , where  $\lambda_d$  is the wavelength of the driving pulse, whereas the single-atom HHG efficiency goes as  $\lambda_d^{-5.5 \pm 0.5}$  [8]. Despite the reduced efficiency, ultrafast sources in the mid-IR are currently exploited to extend the cut-off frequency toward the soft x-ray

region [6]. Moreover, for the generation of isolated attosecond pulses by HHG, few-cycle driver pulses with a stable carrier-envelope phase (CEP) are necessary [9]. Such a feature can be implemented in OPAs by generating the seed pulse through intra-pulse difference frequency generation (DFG) and then amplifying it in a subsequent chain of parametric amplifiers [10, 11].

A large variety in terms of the design of mid-IR OPAs (nonlinear crystal, pump/seed sources etc.) can be found in the literature. Potassium titanyl arsenate (KTA) [12] or periodically-poled lithium niobate (PPLN) [13–15] seem to be the most popular choices for the nonlinear crystals, while the pump source is usually centered around 1  $\mu\text{m}$  exploiting ytterbium [16–18] or neodymium [19] laser drivers. Recently, KTA-based OPAs pumped by Ti:Sapphire lasers were also reported [12, 20, 21]. The latter schemes have followed the same path of amplifying a 1  $\mu\text{m}$  signal in an OPA chain and then producing the mid-IR pulse in the last stage via DFG with the Ti:Sapphire pump. This reduces the detrimental effects of atmospheric water vapor absorption inside the OPA. However, this comes

<sup>4</sup> Author to whom any correspondence should be addressed.

 Original content from this work may be used under the terms of the [Creative Commons Attribution 4.0 licence](https://creativecommons.org/licenses/by/4.0/). Any further distribution of this work must maintain attribution to the author(s) and the title of the work, journal citation and DOI.

with some drawbacks. In collinear interaction geometry an excellent collinear alignment of the pump and the  $1\ \mu\text{m}$  beam, alongside an efficient separation of the amplified signal/idler from the intense pump beam are required. In the case of non-collinear schemes, a well-adjusted angular chirp compensation for the emerging mid-IR idler is necessary. In this work, we present a mid-IR OPA generating pulses tunable between 2.4 and  $3.9\ \mu\text{m}$  with maximum output energy of  $300\ \mu\text{J}$  after compression, a minimum pulse duration after dispersion compensation of less than 60 fs (5 optical cycles at  $3.4\ \mu\text{m}$ ) and passively-stabilized CEP (with residual fluctuations of 240 mrad RMS over 60 s). The OPA is driven by a Ti:Sapphire laser and is based on KTA nonlinear crystals. Comparing with previous schemes, in this case, the mid-IR seed pulse is directly generated by intra-pulse DFG and is then amplified in two OPA stages, without introducing any angular chirp in the output beam. The resulting mid-IR pulse duration is achieved by dispersion compensation in bulk only, preserving the output pulse energy which is then available for experiments. We exploited the short pulse duration and high peak intensity of this OPA source for nonlinear optics experiments in combination with 800 nm laser pulses, demonstrating that this OPA source is perfectly suitable for strong field experiments.

## 2. Description of the OPA source

The experimental setup is depicted in figure 1. It consisted of a three-stage KTA-based quasi-collinear (i.e. with a small angle between the seed and the pump) OPA driven by 1 kHz, 35 fs Ti:Sapphire amplified system (Amplitude Technologies). In total, 5.1 mJ pulses drove the entire OPA. The overall setup was similar to the BBO-based OPA described in [22]. All of the stages used KTA crystals with varying thicknesses of 1, 2 and 3 mm respectively. All these crystals were supplied by Eksma Optics and had a  $12 \times 12\ \text{mm}$  aperture with a broadband anti-reflective coating for 800 nm,  $1\ \mu\text{m}$  and  $3\ \mu\text{m}$ .

In the first step, the mid-IR seed pulses were generated by intra-pulse DFG starting from the 800 nm Ti:Sapphire pulses. Since the bandwidth of our Ti:Sapphire laser is too narrow to generate 3-micron light by intra-pulse DFG, initial spectral broadening was necessary. This was performed in a hollow-core fiber (HCF) filled with Kr at a pressure of 800 mbar by self-phase modulation (SPM). In total, 0.28 mJ of the Ti:Sapphire laser energy was used for this stage. The throughput of the HCF was 57%, resulting in pulses with 0.16 mJ of energy. A short-pass filter was placed after the HCF to cut wavelength components longer than  $1\ \mu\text{m}$  for preventing energy and CEP fluctuations related to spurious nonlinear processes in the amplification stages. After the filter, the ultra-broadband pulses were compressed by multiple bounces on a pair of chirped mirrors ( $-40\ \text{fs}^2$  group delay dispersion each). These pulses have been characterized by second harmonic generation frequency resolved optical gating (SHG-FROG). A near transform-limited pulse duration of 7 fs was achieved after a total of 10 bounces off the two complementary chirped mirrors. The pulses were then focused into a KTA crystal where DFG between the blue and red spectral tails

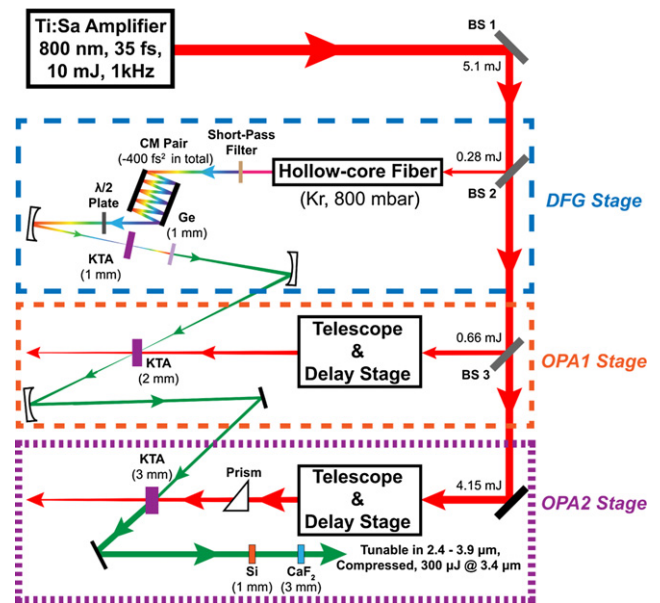


**Figure 1.** Sketch of the experimental setup. An amplified Ti:Sapphire laser drives three stages; the mid-IR seed is obtained by intra-pulse DFG in the first stage and is then boosted in the following two parametric amplification stages (see text for details).

of the driving pulse generated the mid-IR light. We used a 1 mm, type II,  $\theta = 39^\circ$ ,  $\phi = 0^\circ$  crystal. Since the phase-matching condition requires the red and blue components to be cross-polarized, a broadband  $\lambda/2$  plate was used to project the beam polarization on the two crystal axes. The crystal we used has optimal phase-matching around 3500 nm, for this condition the zero GVM is achieved for the DFG process between the 750 nm and 950 nm components of the input pulse. A germanium window (Edmund Optics, 1 mm thickness) after the crystal rejected all the spectral components except for the mid-IR band. The pulse energy of the mid-IR light was estimated to be  $< 1\ \mu\text{J}$ . The beam was then amplified by two OPAs.

The first amplification stage (OPA1) consisted of a 2 mm-thick KTA crystal pumped by 0.66 mJ, 800 nm pulses from the Ti:Sa amplifier. The focal point of the pump was positioned after the crystal to avoid optical damage in the KTA. The mid-IR pulse and the pump beams formed an angle of  $3.3^\circ$ , enabling spatial separation of the beams. The 800 nm pump pulses and the mid-IR amplified pulses have the same horizontal polarization, while the generated one-micron idler pulses have vertical polarization. The output energy of the mid-IR pulse after this stage is  $12\ \mu\text{J}$ .

The second amplification stage (OPA2) was pumped by 4.15 mJ. As in the OPA1 stage, the pump was focused after the crystal. The pump spot size ( $1/e^2$ ) inside the crystal was estimated to be 1.5–2 mm. The angle between the mid-IR pulse and the pump in this stage was  $4.9^\circ$ . This large angle, along with the relatively long propagation distance inside the nonlinear medium, called for the tilting of the pump pulse-front to increase the amplification efficiency. This was obtained by a fused silica prism [23, 24]. The amount of the pulse-front tilt depends on the incidence angle of the pump on the prism. The output energy from the OPA2 stage was  $360\ \mu\text{J}$ . After OPA2 a silicon filter was used for removing all the residual visible

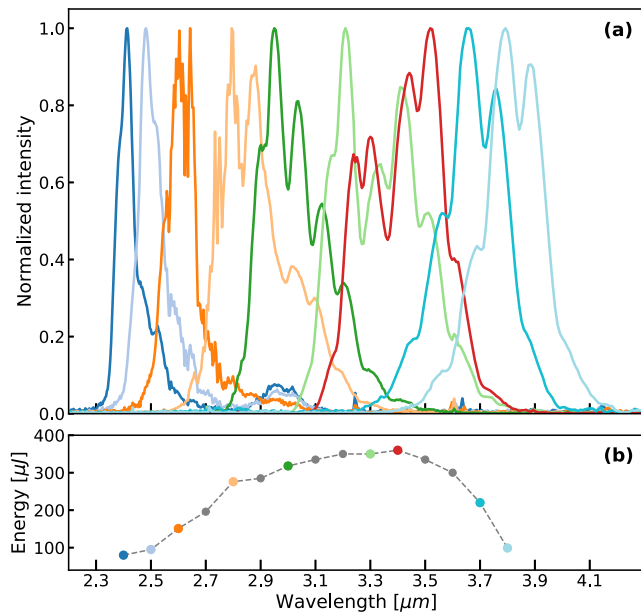


**Figure 2.** (a) Spectral tuning of the OPA source. (b) Corresponding pulse energy for different central wavelengths measured before compression.

light. The pulse was compressed by linear propagation through a plate of  $\text{CaF}_2$ , thanks to its anomalous dispersion in this wavelength region. After compression, the pulse energy at  $3.4 \mu\text{m}$  was about  $300 \mu\text{J}$ . The compression losses were primarily due to the reflection from the surfaces (slight multi-photon absorption losses are also present in the Si plate).

### 3. Characterization of the OPA

Figure 2 shows the tunable spectra obtained from the OPA (measured by a Lasnix FTIR) and the corresponding pulse energies before compression. The spectral modulations visible in figure 2(a) may be attributed to weak reflections inside the KTA crystals and pump-depletion effects in the second amplification stage. As it can be seen, maximum pulse energy of  $360 \mu\text{J}$  was achieved at the central wavelength of  $3.4 \mu\text{m}$ , but energies higher than  $80 \mu\text{J}$  were always obtained across the entire tuning range.

The pulses were characterized by an SHG-FROG exploiting a silver thiogallate (AGS) nonlinear crystal; the measured spectrogram is presented in figure 3(a). A standard iterative pulse retrieval algorithm provided the retrieved spectrogram shown in panel (b); the corresponding pulse intensity envelope and phase in the temporal domain are reported in figure 3(c). The pulse shows an asymmetric envelope, with a slower rise on the leading edge (negative delays). The trailing edge presents a faster slope, with a small plateau at positive delays. The presence of this plateau allowed us to resolve the ambiguity of the sign of the time axis of the FROG trace with an independent two-color HHG measurement in krypton that is discussed later in section 4. Non-linear effects associated with the propagation inside the KTA crystal can contribute to the overall asymmetric shape of the pulse. We also observed an increase in the intensity and duration of the plateau around

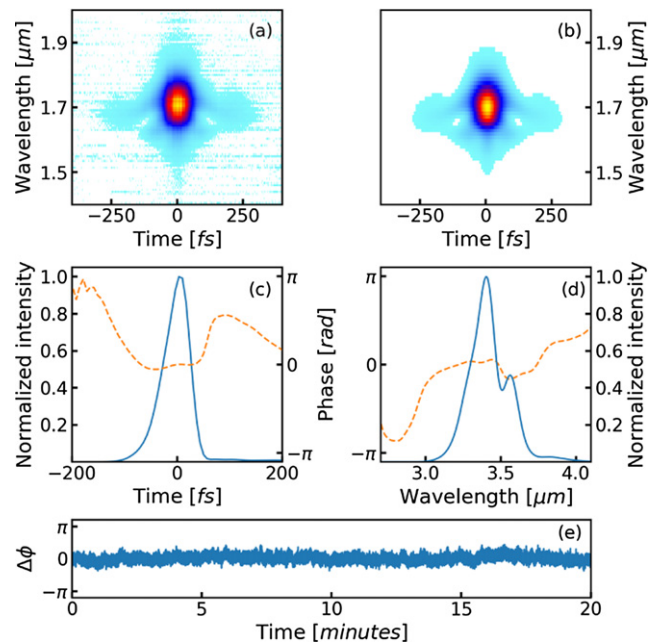


**Figure 3.** Measured (a) and retrieved (b) SHG FROG spectrogram of the mid-IR pulses tuned at  $3.4 \mu\text{m}$ . The retrieved pulse in temporal and spectral domains are reported in panels (c) and (d) respectively. (e) Pulse CEP evolution over a 20 min observation time. Single-shot acquisition; sample rate 75 Hz.

100 fs when the pulse propagates for longer distances in air. This is consistent with the absorption of the radiation from water vapor that is highly effective in this energy range and generates long-lived vibrationally excited states. The overall pulse duration amounts to 56.5 fs, which is close to the transform-limited pulse duration of 49.8 fs. This is also in agreement with the retrieved pulse spectral phase, as reported in figure 3(d), that shows a small residual dispersion across the pulse spectrum.

The output pulse duration amounts to about 5 optical cycles, which is not a usual result in similar KTA-based OPAs, where the typical duration at the output ranges from 70 to 120 fs [12, 20, 21] and nonlinear compression schemes are required to get shorter durations [20]. In order to understand the origin of this outcome we performed numerical simulations of the parametric amplification process inside the last OPA stage in our experimental conditions. The numerical simulations of the OPA were performed starting from an approach developed by the authors [25]. The method is one-dimensional, thus neglecting any effect arising from the transverse structure of the beams, and follows a plane-wave approach. The model solves the nonlinear equation in the frequency domain; as opposed to standard approximate methods, this approach includes the linear dispersion of the medium to all orders, incorporates third-order effects, and does not apply the slowly varying envelope approximation. Figure 4 shows the calculated output pulse bandwidth (a) and the pulse duration (b) after the amplification process in the OPA2 stage as a function of the seed-pump delay at the entrance of the crystal. For increasing delays, the output pulse bandwidth increases from the input value of 4.75 THz up to a maximum value of about 7 THz; the uncompressed pulse duration calculated in

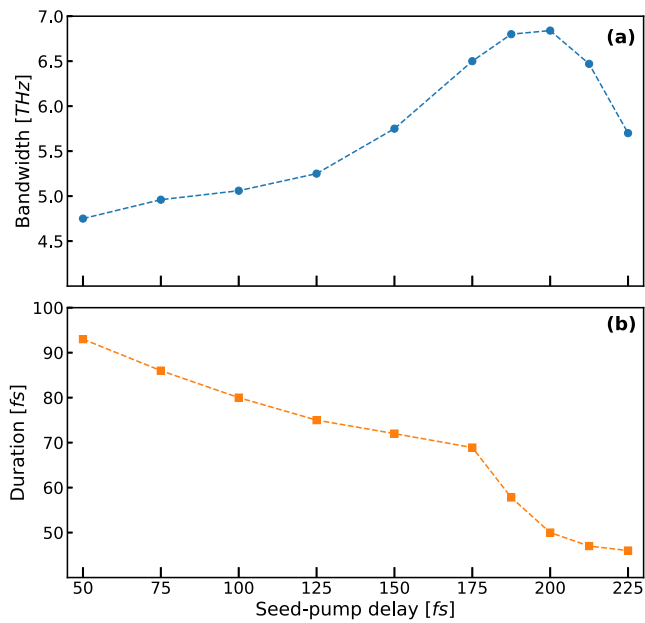


**Figure 4.** Simulated output pulse bandwidth (a) and pulse duration without dispersion compensation (b) as a function of the seed-pump delay at the entrance of the OPA2 crystal. The input seed pulse was calculated from the measured spectrum at the OPA1 output assuming a slightly positive group delay dispersion that takes into account the previous DFG and OPA processes.

this condition is around 50 fs, close to the experimental value. Such result shows that a short temporal duration of the mid-IR seed can be achieved already in the amplification stage when intense pump pulses are exploited and the pump-seed delay is optimized.

Since the OPA is seeded by pulses produced through intra-pulse DFG, the amplified pulses are expected to be CEP-stable. CEP fluctuations in laser sources operating at kHz repetition rates must be characterized shot-by-shot through self-referencing techniques such as  $f-2f$  interferometers. However, the CEP characterization of mid-IR pulses is hampered by the lack of high-resolution spectrometers operating in the 2nd harmonic spectral region (1.3–2  $\mu\text{m}$ ).

For this reason, we opted for the characterization of CEP fluctuations of the second harmonic (SH) of the mid-IR pulses. In this case, the  $f-2f$  measurements can be carried out in the near IR where high-resolution spectrometers are available. The amplitude of the CEP fluctuations of a frequency-doubled pulse train is expected to be twice that of the fundamental pulses.

For the CEP characterization, the OPA was tuned to 3.4  $\mu\text{m}$ ; the mid-IR pulses were frequency-doubled in an AGS nonlinear crystal and the residual mid-IR component was rejected by a band-pass filter; the beam was then sent to an  $f-2f$  interferometer where white light was generated by focusing the pulses in a neodymium-doped yttrium aluminum garnet (YAG) plate. The super-continuum was then focused in a  $\beta$ -barium borate (BBO) nonlinear crystal for second harmonic generation and filtered by a polarizer; the spectral interference pattern was acquired by a spectrometer on a single-shot basis and a suitable Fourier-transform-based analysis was exploited in post-processing for the determination of the CEP fluctuations.

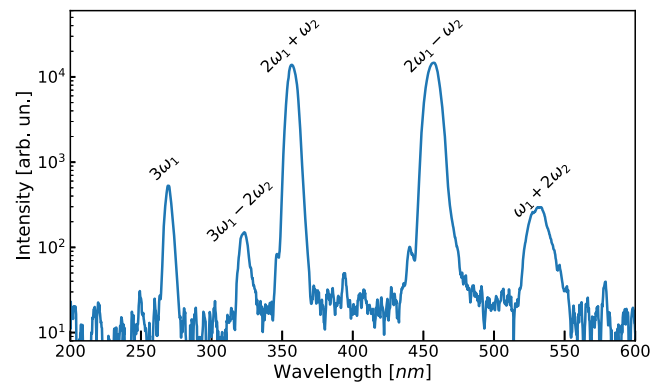


**Figure 5.** Signal generated in air by focusing the mid-IR pulses collinearly combined with the 800 nm pulses from the pump laser. The labels near the main peaks show the corresponding multiphoton processes involved, where  $\omega_1$  and  $\omega_2$  are respectively the central frequencies of the Ti:Sapphire and of the mid-IR pulses.

The CEP evolution of the mid-IR pulses over 20 min, determined as half the measured CEP of the SH pulses, is reported in figure 3(e). The root mean square (rms) of the CEP fluctuation of the OPA beam was about 300 mrad that decreased to 240 mrad in the short term (60 s). The residual long-term CEP drift might be compensated by suitable stabilization systems operating in slow-loop mode acting for instance on the pump-seed delay in the final OPA stage or on the pump intensity.

#### 4. Application of the mid-IR OPA to nonlinear optics and strong field experiments

The developed OPA source is perfectly suitable for investigations in nonlinear optics and strong field science. In order to show its potentialities, we combined the mid-IR pulses tuned at  $\lambda_2 = 3.2 \mu\text{m}$  with the pulses at  $\lambda_1 = 800 \text{ nm}$  from the pump laser. A dichroic beam combiner with high transmission for the OPA pulses and high reflection for the Ti:Sapphire pulses was exploited. In our experiments the two pulses were polarized along the horizontal direction and were synchronized with a high-precision delay line.

In a first proof-of-concept experiment, the pulses had the same energy of about 150  $\mu\text{J}$  and were focused in air by a spherical mirror with 15 cm focal length. The radiation emerging from the interaction region was analyzed with a spectrometer operating from the UV to the visible region. The resulting spectrum is reported in figure 5 in logarithmic scale. Several peaks appear due to four-wave (FWM) and six-wave (SWM) mixing processes, as indicated by the labels at each peak. Besides the third harmonic of the Ti:Sapphire pulses at  $\omega = 3\omega_1$ , two intense FWM peaks appear at  $\omega = 2\omega_1 \pm \omega_2$ . A weaker peak is also visible at  $\omega = \omega_1 + 2\omega_2$ . The peak intensity of the mid-IR pulses is sufficient to promote SWM processes, as proven by the appearance of a peak at  $\omega = 3\omega_1 - 2\omega_2$ .

We also performed a two-color HHG experiment. We generated harmonics by focusing the two-color driving field into a pulsed gas jet of krypton, with a backing pressure of 3 bar. The pulsed jet is produced by a solenoid valve with a 500  $\mu\text{m}$

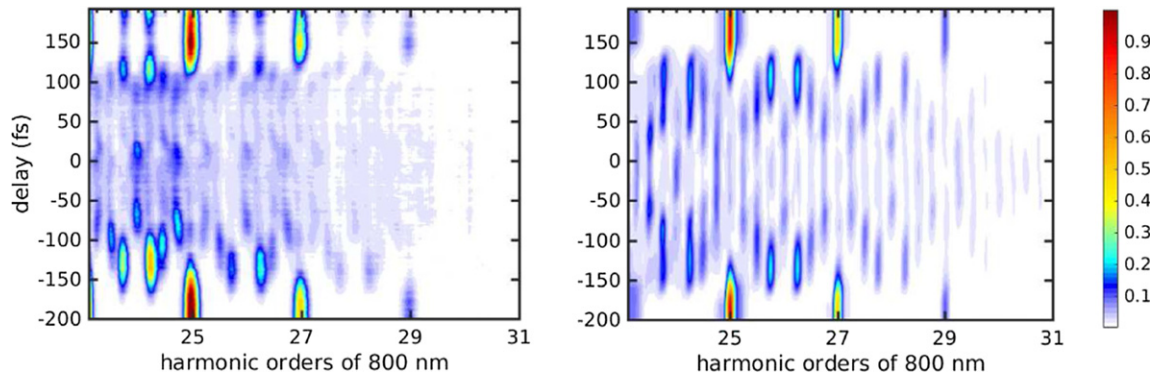


**Figure 6.** (a) Evolution of HHG spectra in krypton as a function of the delay between  $3.25 \mu\text{m}$  and  $800 \text{ nm}$  pulses. (b) Theoretical simulation of HHG spectra generated in the experimental condition corresponding to (a); positive delays correspond to the mid-IR pulse arriving later with respect to the NIR pulse.

nozzle working at 20 Hz repetition rate. The harmonic spectra were acquired by a flat-field XUV spectrometer coupled with a detector composed of a micro-channel plate, a phosphor screen and a CCD camera. The mid-IR pulses had an on-target energy of  $70 \mu\text{J}$ , whereas the  $800 \text{ nm}$  pulses had a duration of about  $50 \text{ fs}$  and an energy of about  $170 \mu\text{J}$ . Figure 6(a) shows HHG spectra generated by the two-color field as a function of the delay between the two color components. We observed a spectral modulation in the region of temporal overlap between the two components. In particular, we observed the appearances of several spectral features. These features can be associated to the non-linear mixing of the interacting photons in the medium. For understanding the mechanism behind this process, we performed single active electron simulations based on Lewenstein's model [26]. Since in the experiment we acquired HHG spectra averaged over 400 laser shots, in the simulations we averaged over the CEP random fluctuations of the  $800 \text{ nm}$  component accordingly. The simulation results are reported in figure 6(b) and show a good agreement with the experimental observations. From this calculation, it is possible to assign each feature in the HHG spectra to the proper multiphoton process. For instance, at large delays between the two pulses, we observed only the odd harmonics of the  $800 \text{ nm}$  field. As the pulses' overlap begins (around  $-120 \text{ fs}$ ) we observed between each harmonic of the  $800 \text{ nm}$  field the appearance of two strong peaks, corresponding to  $\omega = n\omega_1 \pm \omega_2$  with even  $n$ , and two weaker peaks, corresponding to  $\omega = m\omega_1 \pm 2\omega_2$  with odd  $m$ . These results are consistent with the ones we obtained for the mixing in air with  $n = 2$  and  $m = 1, 3$ . When the delay between the two pulses becomes shorter, new spectral components appear as a result of the activation of higher-order nonlinear processes. For instance, around  $-70 \text{ fs}$  we observed the appearance of three new peaks between the odd harmonic of the  $800 \text{ nm}$  component, corresponding to  $\omega = m\omega_1 \pm 4\omega_2$  (central peak) and  $\omega = n\omega_1 \pm 3\omega_2$  (outer peaks). At  $200 \text{ fs}$ , an interaction between the two colors can still be observed in the experiment, while no interaction is observed at the corresponding negative value of  $-200 \text{ fs}$ . This is ascribed to the asymmetric shape of the mid-IR envelope that has not been taken into account in the simulation. The presence of this signal confirms that the plateau observed in the FROG retrieval can be associated with the trailing edge of the mid-IR pulse.

The overall agreement between the calculations and the experimental results supports the interpretation of these spectral features as manipulation of the electron trajectories by the combination of the two laser pulses in the framework of strong field approximation (SFA) [26].

## 5. Conclusion


We developed a mid-IR ultrafast OPA tunable between  $2.4$  and  $3.9 \mu\text{m}$  providing few-cycle pulses with a near transform-limited pulse duration of less than  $60 \text{ fs}$  (5 optical cycles at  $3.4 \mu\text{m}$ ) and maximum output energy of  $300 \mu\text{J}$  after compression. A passive stabilization scheme was implemented allowing to achieve a CEP with an RMS noise of about  $300 \text{ mrad}$  over  $20 \text{ min}$ . The energy efficiency of the reported OPA (pump energy vs output energy of the mid-IR beam after compression) is  $5.9\%$ , which is higher than other results found in the literature for Ti:Sapphire-pumped KTA schemes [12, 20, 21]. The performances of the reported OPA in terms of efficiency and output pulse duration is also competitive with several results involving PPLN crystals and one-micron pumps [15, 17, 18]. Overall, the presented mid-IR OPA proposes a robust and compact scheme for generating CEP-stable mid-IR pulses for strong-field physics applications, when a Ti:Sapphire driving laser is already available.

Proof-of-concept investigations have been performed, showing that this OPA source can be effectively used in nonlinear optics experiments, such as FWM and two-color HHG. In particular, the latter experiment and its interpretation with SFA calculations demonstrate the capabilities of this mid-IR source to manipulate electron trajectories. Thus this OPA is very well suited for HHG spectroscopy experiments [27].

## Acknowledgments

This study was supported by the European Union's Horizon 2020 research and innovation program under the Marie Skłodowska-Curie projects MEDEA (Grant No. 641789) and ASPIRE (Grant No. 674960), by the European Research Council Starting Research Grant UDYNI (Grant No. 307964), by the Italian Ministry of Research and Education (ELI project-ESFRI Roadmap).

## ORCID iDs

Prabhash Prasannan Geetha  <https://orcid.org/0000-0003-4051-368X>

Davide Faccialà  <https://orcid.org/0000-0002-5072-0394>

Anna G Ciriolo  <https://orcid.org/0000-0003-1189-329X>

Michele Devetta  <https://orcid.org/0000-0002-3806-3475>

Caterina Vozzi  <https://orcid.org/0000-0002-0212-0191>

## References

- [1] Woutersen S, Emmerichs U and Bakker H J 1997 *Science* **278** 658–60
- [2] Dormidonov A, Kompanets V, Chekalin S and Kandidov V 2015 *Opt. Express* **23** 29202–10
- [3] Malevich P N et al 2015 *Opt. Lett.* **40** 2469–72
- [4] Herbst J, Heyne K and Diller R 2002 *Science* **297** 822–5
- [5] Shambhu G and Reis David A 2019 *Nat. Phys.* **15** 10–6
- [6] Popmintchev T et al 2012 *Science* **336** 1287–91
- [7] Wolter B et al 2016 *Science* **354** 308–12
- [8] Colosimo P et al 2008 *Nat. Phys.* **4** 386
- [9] Calegari F, Sansone G, Stagira S, Vozzi C and Nisoli M 2016 *J. Phys. B: At. Mol. Opt. Phys.* **49** 062001
- [10] Baltuška A, Fuji T and Kobayashi T 2002 *Phys. Rev. Lett.* **88** 4
- [11] Vozzi C, Calegari F, Benedetti E, Gasilov S, Sansone G, Cerullo G, Nisoli M, De Silvestri S and Stagira S 2007 *Opt. Lett.* **32** 2957
- [12] Chen Y, Li Y, Li W, Guo X and Leng Y 2016 *Opt. Commun.* **365** 7–13
- [13] Brida D, Marangoni M, Manzoni C, Silvestri S D and Cerullo G 2008 *Opt. Lett.* **33** 2901–3
- [14] Bigler N, Pupeikis J, Hrisafov S, Gallmann L, Phillips C R and Keller U 2018 *Opt. Express* **26** 26750–7
- [15] Fu Y, Xue B, Midorikawa K and Takahashi E J 2018 *Appl. Phys. Lett.* **112** 241105
- [16] Thire N, Maksimenka R, Kiss B, Ferchaud C, Bizouard P, Cormier E, Osvay K and Forget N 2017 *Opt. Express* **25** 1505–14
- [17] Heiner Z, Petrov V, Steinmeyer G, Vrakking M J J and Mero M 2018 *Opt. Express* **26** 25793–804
- [18] Ishii N, Xia P, Kanai T and Itatani J 2019 *Opt. Express* **27** 11447–54
- [19] Elu U, Baudisch M, Pires H, Tani F, Frosz M H, Köttig F, Ermolov A, Russell P S and Biegert J 2017 *Optica* **4** 1024–9
- [20] Lu F, Xia P, Matsumoto Y, Kanai T, Ishii N and Itatani J 2018 *Opt. Lett.* **43** 2720–3
- [21] He H et al 2018 *Appl. Phys. B* **124** 31
- [22] Vozzi C et al 2006 *Opt. Express* **14** 10109
- [23] Hebling J 1996 *Opt. Quantum Electron.* **28** 1759–63
- [24] Akturk S, Gu X, Zeek E and Trebino R 2004 *Opt. Express* **12** 4399
- [25] Cirmi G, Manzoni C, Brida D, De Silvestri S and Cerullo G 2008 *J. Opt. Soc. Am. B* **25** B62–9
- [26] Lewenstein M, Balcou P, Ivanov M Y, L’Huillier A and Corkum P B 1994 *Phys. Rev. A* **49** 2117–32
- [27] Faccialà D et al 2016 *Phys. Rev. Lett.* **117** 093902